Mitochondria and calcium defects correlate with axonal dysfunction in *GDAP1*-related Charcot-Marie-Tooth mouse model

Azahara Civera-Tregón [a,b,1], Laura Domínguez [a,b], Paula Martínez-Valero [c,2], Clàudia Serrano [a,d,3], Alex Vallmitjana [d,4], Raúl Benítez [d], Janet Hoenicka [a,b], Jorgina Satrústegui [b,c], Francesc Palau [a,b,e,f,*]

[a] *Laboratory of Neurogenetics and Molecular Medicine – IPER, Institut de Recerca Sant Joan de Déu, Barcelona, Spain*
[b] *Centro de Investigación Biomédica en Red de Enfermedades Raras (CIBERER), Barcelona, Madrid, Spain*
[c] *Departamento de Biología Molecular, Centro de Biología Molecular Severo Ochoa (CBMSO), Consejo Superior de Investigaciones Científicas – Universidad Autónoma de Madrid, Madrid, Spain*
[d] *Biomedical Engineering Research Center, Universitat Politècnica de Catalunya and Institut de Recerca Sant Joan de Déu, Barcelona, Spain*
[e] *Department of Genetic and Molecular Medicine – IPER, Hospital Sant Joan de Déu, Barcelona, Spain*
[f] *Clinic Institute of Medicine and Dermatology, Hospital Clínic, and Division of Pediatrics, Faculty of Medicine and Health Sciences, University of Barcelona, Barcelona, Spain*

ARTICLE INFO

ABSTRACT

Ganglioside-induced differentiation associated protein 1 (*GDAP1*) gene encodes a protein of the mitochondrial outer membrane and of the mitochondrial membrane contacts with the endoplasmic reticulum (MAMs) and lysosomes. Since mutations in *GDAP1* cause Charcot–Marie–Tooth, an inherited motor and sensory neuropathy, its function is essential for peripheral nerve physiology. Our previous studies showed structural and functional defects in mitochondria and their contacts when GDAP1 is depleted. Nevertheless, the underlying axonal pathophysiological events remain unclear. Here, we have used embryonic motor neurons (eMNs) cultures from *Gdap1* knockout (*Gdap1*$^{-/-}$) mice to investigate in vivo mitochondria and calcium homeostasis in the axons. We imaged mitochondrial axonal transport and we found a defective pattern in the *Gdap1*$^{-/-}$ eMNs. We also detected pathological and functional mitochondria membrane abnormalities with a drop in ATP production and a deteriorated bioenergetic status. Another consequence of the loss of GDAP1 in the soma and axons of eMNs was the in vivo increase calcium levels in both basal conditions and during recovery after neuronal stimulation with glutamate. Further, we found that glutamate-stimulation of respiration was lower in *Gdap1*$^{-/-}$ eMNs showing that the basal bioenergetics failure jeopardizes a full respiratory response and prevents a rapid return of calcium to basal levels. Together, our results demonstrate that the loss of GDAP1 critically compromises the morphology and function of mitochondria and its relationship with calcium homeostasis in the soma and axons, offering important insight into the cellular mechanisms associated with axonal degeneration of *GDAP1*-related CMT neuropathies and the relevance that axon length may have.

1. Introduction

Charcot-Marie-Tooth (CMT) disease is a genetic neurodegenerative disorder of the peripheral nervous system (PNS) characterized by distal muscle weakness and atrophy, distal sensory loss and limbs deformities (Pareyson et al., 2017). CMT genes mutations cause demyelinating or axonal forms of the disease, and the pathogenic mechanisms comprise a wide-range of biological processes and pathways that affect motor neurons (MNs) in the spinal cord (Rossor et al., 2013). Mutations in the *Ganglioside-induced differentiation-associated protein 1* gene (*GDAP1*)

cause CMT associated with several phenotypes including autosomal recessive demyelinating (CMT4A) (Baxter, 2002), autosomal recessive axonal (AR-CMT2K) (Cuesta et al., 2002) and autosomal dominant axonal (CMT2K) (Claramunt et al., 2005; Sivera et al., 2010).

GDAP1 is an atypical transmembrane glutathione S-transferase (GST) (Marco et al., 2004) of the mitochondrial outer membrane (MOM) (Niemann et al., 2005; Pedrola et al., 2005) and has been described as a fission factor regulating mitochondrial dynamics (Niemann et al., 2009). GDAP1 is also located in mitochondria-associated membranes (MAMs) (Pla-Martín et al., 2013), which are specialized subdomains of membrane contact sites between the ER and mitochondria (Naon and Scorrano, 2014). In cellular models, the pathophysiology of GDAP1 includes structural defects in mitochondria, the mitochondrial network, ER, MAMs (Pla-Martín et al., 2013) and in the membrane contact sites (MCSs) between mitochondria and lysosomes (Cantarero et al., 2020). The *Gdap1* knockout mouse (*Gdap1$^{-/-}$*) shows loss of motor neurons and abnormal neuromuscular junctions (Barneo-Munoz et al., 2015), and induces an inflammatory response in the spinal cord and sciatic nerve (Fernandez-Lizarbe et al., 2019). In addition, GDAP1 depletion causes oxidative stress (Niemann et al., 2009; Noack et al., 2012) and failure in calcium (Ca^{2+}) signaling associated to store-operated Ca^{2+} entry (SOCE) activity (Barneo-Munoz et al., 2015; Pla-Martín et al., 2013). However, very little is known about the axon pathophysiology of the *GDAP1*-related neuropathies.

Mitochondria provide the energy necessary to support neuronal functions and axonal physiology including growth and branching of axons and synaptic functions. Proper mitochondrial trafficking within the axons is of utmost importance in physiology and disease (Li et al., 2020). Mitochondrial axonal transport is affected in dorsal root ganglia (DRG) neurons expressing mutated forms of the mitochondrial MFN2 protein in CMT disease (Baloh et al., 2007). On the other hand, clinical studies suggest that the length of the nerves is relevant in the pathophysiology in patients with *GDAP1*-related CMT (Sevilla et al., 2008). Mitochondria also have an impact on Ca^{2+} signals and homeostasis in the cytosol and mitochondria (Brini et al., 2014) especially during and after neuronal stimulation for a rapid synaptic recovery and synaptic transmission preservation (Devine and Kittler, 2018; Vos et al., 2010). Mitochondrial Ca^{2+} in both the matrix and the intermembrane space is important to upregulate mitochondrial function (Denton, 2009; Satrustegui et al., 2007) and maintain adequate ATP production to support synaptic function (Satrustegui et al., 2007). Indeed, Ca^{2+} ions activate NADH shuttle systems in the outer face of the inner mitochondrial membrane and matrix Krebs cycle dehydrogenases, thereby stimulating oxidative phosphorylation in neurons (Denton, 2009; Glancy and Balaban, 2012; Llorente-Folch et al., 2013).

In this work, we used cultured embryonic motor neurons (eMNs) of the spinal cord from a *Gdap1$^{-/-}$* mouse to gain an in-depth understanding of the mitochondrial and calcium homeostasis defects that could cause peripheral axonopathy in this model of disease (Barneo-Munoz et al., 2015). We find that the lack of GDAP1 led to a marked disruption of axonal mitochondrial transport, impairs mitochondrial membrane potential and respiratory chain function, and causes a Ca^{2+} dyshomeostasis in the soma and axons with an abnormal response of eMNs to glutamate. These results help to explain the complex pathophysiology of *GDAP1*-related CMT neuropathies and the relevance that axon length may have.

2. Material and methods

2.1. Animals and embryonic motor neuron primary culture

Gdap1 knockout (*Gdap1$^{-/-}$*) mice were previously generated and characterized in our laboratory (Barneo-Munoz et al., 2015). All the animals were kept under controlled temperature (23 °C) and humidity (60%) on a 12 h light/dark cycle with access to food and water ad libitum. Principles of laboratory animal care and the animal facility

(NIH publication No. 86-23, revised 1985) were followed, as well as the current version of the European Union Council guidelines (2010/63/EU) and Spanish law (RD 1201/2005). Experimental procedures were approved by the Animal Experimental Ethics Committee (CEEA) of the University of Barcelona (registration no. C-133/18 [10071], Government of Catalonia). The genotype of the mice was confirmed for each of the male-female pairing from which the embryos were obtained. eMNs cultures were prepared from 13.5 embryonic day (E13.5) mouse spinal cord as previously described (Gingras et al., 2007) with some modifications (Barneo-Munoz et al., 2015). Briefly, mouse embryo spinal cords were dissected and the dorsal half removed. Ventral spinal cords were dissociated mechanically after trypsin treatment (0.025% trypsin in HBSS) and collected afterward under a 4% bovine serum albumin (BSA) cushion. The largest cells were isolated by centrifugation (10 min at 520*g*) using iodixanol density gradient purification. The collected cells were finally suspended in a tube containing eMN complete medium: Neurobasal (Life technologies) supplemented with B27 (Life technologies), 2% horse serum (Life technologies), 1× glutamax (Life technologies), and a cocktail of recombinant neurotrofins: 1 ng/mL BDNF, 10 ng/mL GDNF, 10 ng/mL CNTF, and 10 ng/mL HGF (PreProtech). Isolated eMNs were plated on poly-D-lysine/laminin-coated surfaces as described previously (Soler et al., 1998), and grown in a 5% CO_2 incubator at 37 °C. Media was changed every 2–3 days and 2 μM AraC (Sigma-Aldrich) was added to the culture medium to limit the growth of non-neuronal cells. Cultured eMNs were identified by morphological criteria. All experiments were performed between DIV3-DIV5, except neuronal survival experiments that were done at DIV7.

2.2. Measurement of mitochondrial axonal transport

In-vivo mitochondrial movement in eMNs was studied using microfluidic chambers, which are composed of two open culture chambers connected by a parallel array of microchannels. The system allows fluidic separation of axons from the soma and permits observing mitochondrial movement along oriented axons. Microfluidic chambers were prepared as previously described (Southam et al., 2013). On the day of the experiment, eMNs were loaded with 100 mM MitoTracker Green (MTG, mitochondria-specific dye, Thermo Fisher Scientific) for 30 min at 37 °C in HCSS medium, 2.5 mM glucose, 2 mM Ca^{2+}. 8-bits fluorescence images were acquired every 5 s for 150 s in live neuronal imaging through 488 nm excitation wavelength using a 20x objective (zoom of 2) on a Leica SP2 confocal microscope (Leica Microsystems).

An automatic image processing pipeline was developed to analyze mitochondrial axonal transport from time-lapsed fluorescence microscopy images. The pipeline is described in detail in Vallmitjana et al. (Vallmitjana et al., 2017), but here we give a brief description of the video tracking algorithm. To remove background noise and smooth surfaces for object segmentation, each frame was preprocessed with spatial Gaussian filtering with a standard deviation σ = 0.33 um. Mitochondria were segmented in each frame using a two-step process. Initially, using a custom watershed segmentation algorithm that included a stopping rule enforcing a required minimum area and normalized intensity of the detected candidates of 1 μm^2 and 0.2 μm^2, respectively. This initial coarse segmentation provided the grounds for a more detailed measuring of shape and size for each candidate. Segmentation accuracy was further enhanced by a rule-based merging and filtering algorithm that fused over-segmented mitochondria and removed spurious objects. A probabilistic feature-based tracking was used to identify mitochondrial trajectories. The probabilistic model described the position and velocity of each object at a particular frame conditional to their properties in previous frames. A maximum-at-posterior estimation of the model allowed to establish a temporal connection of the segmented mitochondria and determine their trajectories. Subsequent trajectory analysis was applied to correct misallocated points and fix truncated trajectories. As a final stage, feature extraction was used to characterize the time-averaged properties of both

static objects (area, major axis length, axis length ratio, max pixel intensity) and trajectories (velocity, distance traveled and direction of movement -anterograde or retrograde-).

2.3. Electron microscopy

For Transmission Electron Microscopy (TEM) eMNs were seeded onto poly-D-lysine/laminin-coated Lab-Tek chamber slides (Nalge Nunc International) at 6.000 cells/well density, fixed in 2.5% glutaraldehyde for 1 h at 37 °C and subsequently processed for TEM as previously reported (Voliani et al., 2013). Two non-overlapping regions (16.500 magnification) containing numerous mitochondria were selected for each eMN. For mitochondria morphology analysis, we calculated the ratio of mitochondria with lamellar or disorganized (ballooned and swollen) cristae to the total number of mitochondria per field. For mitochondria-ER contacts analysis, we quantified the number of mitochondria displaying close contacts with ER and expressed it relative to the total number of mitochondria per field.

2.4. Measurement of mitochondrial membrane potential ($\Delta\psi_m$)

Mitochondrial membrane potential was measured using the fluorescence probe 5,5′,6,6′-tetrachloro-1,1′,3,3′ tetraethylbenzimidazolylcarbocyanine iodide (JC-1), which accumulates in mitochondria depending on the $\Delta\psi m$. eMNs were plated at 12,000 cells/well onto 12 mm round coverslips. eMNs were load with 3 μM JC1 dye (Thermo Fisher Scientific) in HCSS medium, 2.5 mM glucose, 2 mM Ca^{2+} for 30 min at 37 °C. The emission of JC-1 monomers and aggregates were detected in live neuronal imaging through 530–550 nm and 585–650 nm emission wavelength ranges respectively. 12-bits fluorescence images were acquired in live neuronal imaging using a 20x objective (zoom of 2.5) on a Leica TCS-SP8 X White Light Laser confocal microscope (Leica Microsystems). To quantify $\Delta\psi_m$, fluorescence intensity relative to the area was measured in neuronal somas with ImageJ 1.51u software (from National Institutes of Health) and the fluorescence ratio 590 nm/530 nm was expressed.

2.5. Measurement of cellular oxygen consumption

Cellular oxygen consumption rate (OCR) was measured using a Seahorse XF24 Extracellular Flux Analyzer (Seahorse Bioscience; (Qian and Houten, 2010)). eMNs were plated in XF24 V7 cell culture at 40.000 cells/well and incubated in a 37 °C, 5% CO_2 incubator. The instrument was calibrated the day before the experiment, following the manufacturer's instructions. On the day of the experiment, cultures were preconditioned for 1 h (during the sensor calibration) in HCSS medium (120 mM NaCl, 0.8 MgCl$_2$, 25 mM HEPES, 5.4 mM KCl, pH 7.4), 2.5 mM glucose, 2 mM Ca^{2+} and maintained in a 37 °C incubator without CO_2. eMNs were also maintained in the same medium during respirometry experiments. Mitochondrial function in eMNs was determined through sequential addition of electron transport chain inhibitors: 6 μM oligomycin, 1.6 mM 2,4- dinitrophenol, and 1 μM antimycin A/1 μM rotenone. OCR was normalized to total protein/well and calculated as OCR-$OCR_{A/R}$ to subtract non-mitochondrial respiration. ATP-linked respiration was calculated as OCR-OCR_{olig}. Non-ATP linked oxygen consumption was calculated as OCR_{olig}-$OCR_{A/R}$. Maximal uncoupled respiration was calculated as OCR_{MUR}-$OCR_{A/R}$. For mitochondrial respiration in response to Ca^{2+-} mobilizing agents we used 25 μM glutamate, 250 μM carbachol, 100 μM ATP, 25 μM NMDA and 10 μM dantrolene (Sigma-Aldrich).

2.6. Measurement of mitochondrial ATP

Total intracellular ATP levels were measured using the CellTiter-Glo® Luminescent Cell Viability assay kit (Promega), according to the manufacturer's instruction. eMNs were seeded in a 96-well cell culture plate at 25,000 cells/well. To specifically quantify the mitochondrial ATP levels, some wells were treated with 6 μM oligomycin for 15 min at 37 °C before performing the luminescence experiment, to block oxidative phosphorylation and thus the ATP produced in that process. Mitochondrial ATP levels were calculated by subtracting the luminescent signal of oligomycin treated eMNs from the luminescence signal of untreated eMNs. For the detection of a luminescent signal, CellTiter-Glo reagent was added and luminescence was measured in the GloMax® Navigator Microplate Luminometer (Promega).

2.7. Calcium imaging

Cytosolic Ca^{2+} ($[Ca^{2+}]_{cyt}$) imaging was performed with Fura-2 AM (cytosolic Ca^{2+}-ratiometric fluorescent dye, Thermo Fisher Scientific) as previously described (Ruiz et al., 1998). eMNs were plated at 12,000 cells/well onto 12 mm round coverslips and loaded with 5 μM Fura-2 AM and pluronic acid F.127 0.06% (Sigma-Aldrich) for 30 min at 37 °C in Ca^{2+}-free HCSS medium with 2.5 mM glucose and washed for 30 min in HCSS medium, 2 mM CaCl$_2$, 2.5 mM glucose. Loaded cells were visualized using a Leica DMI6000 Microscope with a 40x oil-immersion objective and images were acquired at 5 s intervals for 5 min. Fura-2 AM fluorescence was imaged ratiometrically using alternate excitation at 340 and 380 nm, and a 510 nm emission filter. Regions of interest (ROIs) were selected by morphology taking into account only eMNs. Fluorescence emission (510 nm) ratio of Ca^{2+}-free (F380) to Ca^{2+}-free bound probe (F340) was analyzed using Metafluor for Leica developed by Metamorph (Universal Imaging). $[Ca^{2+}]_{cyt}$ was calculated from ratio fluorescence Fura-2 AM measurements following an intracellular calibration procedure according to the Grynkiewicz equation (Grynkiewicz et al., 1985). Ca^{2+}-signals during excitatory stimulation were monitored following exposure to 25 μM glutamate applied as a bolus 30 s later, eMNs were perfused continuously with glutamate-free solution (HCSS medium, 2 mM CaCl2, 2.5 mM glucose) using a peristaltic pump for additional 4 min to recover basal cytosolic Ca^{2+} levels.

2.8. Western blotting

Cultured eMNs growing in poly-L-lysine and laminin-coated 6-well cell culture plate at 600,000 cells/well were lysed in a lysing buffer containing: 50 mM Tris- HCl (pH 7.4), 1.5 mM MgCl$_2$, 5 mM EDTA, 1% Triton-X100, 50 mM NaF and 1 Mm Na$_2$VO$_3$ supplemented with a protease inhibitor mixture (Roche Molecular Biochemical). Protein concentration was determined using the BCA kit (Pierce). Equal amounts of proteins (30 μg) of each sample were loaded onto SDS-polyacrylamide gels and transferred to a polyvinylidene fluoride membrane (EMD Millipore). Membranes were blocked with 5% dried milk or 5% BSA (Sigma-Aldrich) for phosphorylated proteins in TBS containing 0.1% Tween-20 (Sigma-Aldrich) and then incubated overnight at 4 °C using the following antibodies: α-phospho eIF2α (1:100), α-eIF2α (1:100), α-BIP (1:100), α-CHOP (1:250), α-Cleaved Caspase-3 (1:100) from Cell Signaling, α-GRP94 (1:1000) from Abcam and α-β-Tubulin III (1:15,000) from Sigma-Aldrich. After washing, blots were incubated with a goat α-rabbit peroxidase-conjugated IgG or goat α-mouse peroxidase-conjugated IgG (1:10,000; Abcam) for 1 h at room temperature. Proteins were processed for chemiluminescence with Amersham ECL Prime Western Blotting Detection Reagent and visualized by iBright™ CL1000 Imaging System (Thermo Fisher Scientific). Bands intensity was measured through the total area of the peaks using the AlphaImager2200 software (Alpha Innotech Corporation). For endoplasmic reticulum-stress experiments, neurons were treated with thapsigargin (Sigma-Aldrich) 0.1 μM for 18 h.

2.9. Statistical analysis

Statistical analysis was performed using the GraphPad Prism 8.0.2 software (GraphPad Software). The normal distribution of data was

calculated with the Kolmogorov-Smirnov normality test. To determine significant values between different experimental groups, the mean data were compared using unpaired Student's two-tailed *t*-test for Gaussian-distributed data and non-parametric Mann-Whitney-*U* test for no Gaussian-distributed data. The results were represented as means and standard error of the mean (SEM). Significant *p-values:* *$p < 0.05$; **$p < 0.01$; ***$p < 0.001$ were considered.
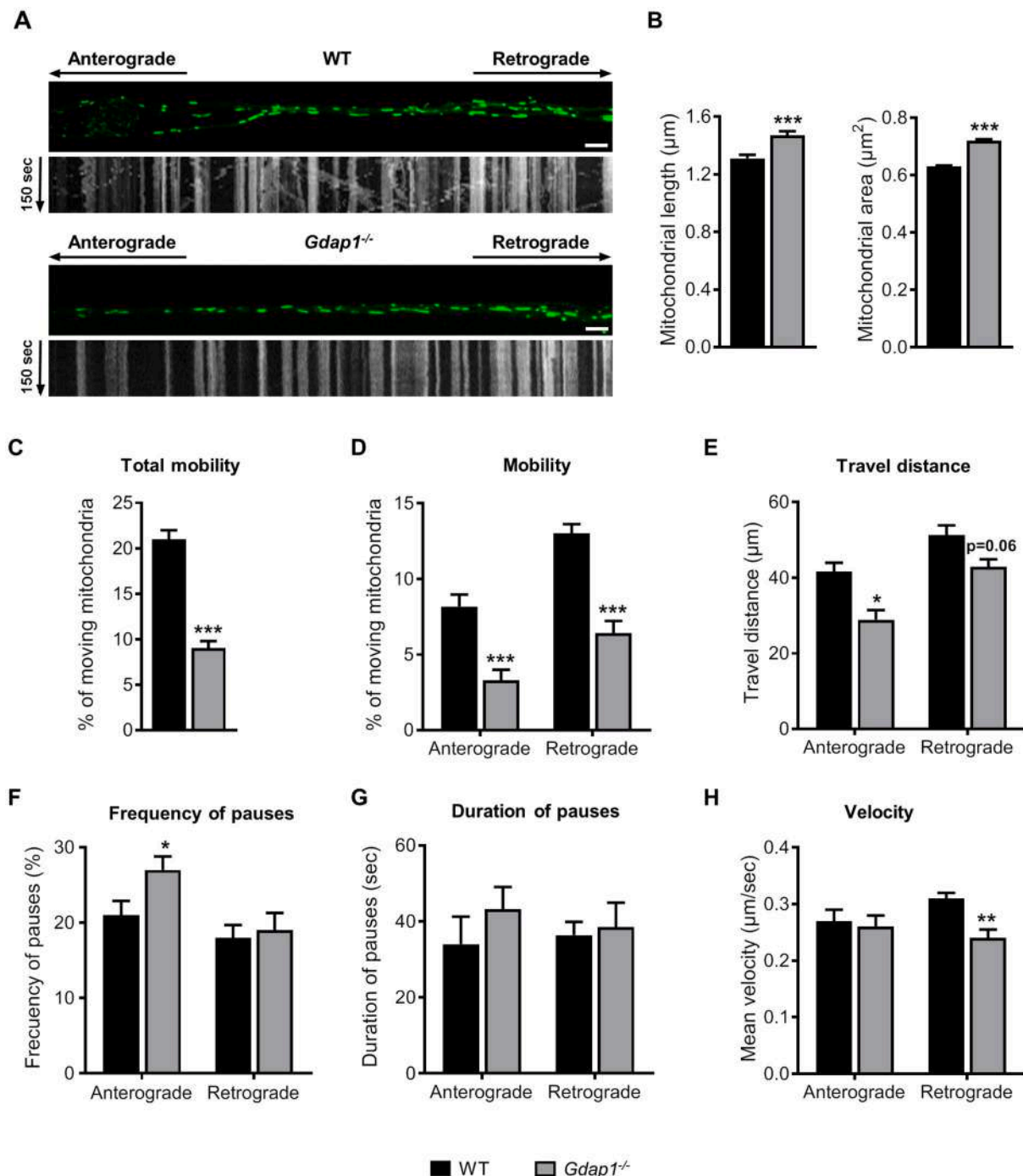

Fig. 1. Loss of GDAP1 disrupts mitochondrial axonal transport in eMNs. (A) Representative images of mitochondria morphology and kymographs showing mitochondrial axonal transport in wild-type (WT) and *Gdap1*$^{-/-}$ eMNs. (B) Mitochondrial morphology analysis revealed that mitochondria length and area were increased in *Gdap1*$^{-/-}$ eMNs compare with WT eMNs. n (mitochondria) = 1896 WT, 1214 *Gdap1*$^{-/-}$. (C) Live imaging analysis showed that in the absence of GDAP1 the percentage of total moving mitochondria is significantly reduced. n (axons) = 38 WT, 30 *Gdap1*$^{-/-}$. (D) The percentage of anterograde and retrograde moving mitochondria was reduced in *Gdap1*$^{-/-}$ compared to WT eMNs. n (axons) = 38 WT, 30 *Gdap1*$^{-/-}$. (E) The average travel distance was reduced in *Gdap1*$^{-/-}$ eMNs in both anterograde and retrograde transports, but the retrograde travel distance did not reach statistical significance ($p = 0.06$). (F) Frequency of pauses was only reduced in anterograde transport, (G) but no differences were found in pauses duration in either of transports. n (anterograde moving mitochondria) = 155 WT, 40 *Gdap1*$^{-/-}$. n (retrograde moving mitochondria) = 247 WT, 78 *Gdap1*$^{-/-}$. (H) Quantification of mitochondria velocity in both anterograde and retrograde movements showing that only the retrograde movement velocity was reduced. n (anterograde moving mitochondria) = 155 WT, 40 *Gdap1*$^{-/-}$. n (retrograde moving mitochondria) = 247 WT, 78 *Gdap1*$^{-/-}$. Data are expressed as mean ± SEM from three independent experiments. *$p \leq 0.05$, **$p \leq 0.01$, ***$p \leq 0.001$. Scale bars: 5 μm.

3. Results

3.1. Lack of GDAP1 causes defective mitochondrial axonal transport in eMNs

Efficient mitochondrial transport is of utmost importance in neurons to supply mitochondria into synapses where there is a high demand for energy and calcium buffering (Lin and Sheng, 2015). To investigate the role of GDAP1 in axon mitochondrial physiology, we studied the morphology and transport of mitochondria using time-lapse confocal live imaging in cultured eMNs of $Gdap1^{-/-}$ and wild-type mice (Fig. 1a, Supplementary Videos 1 [KO] and 2 [WT]). In $Gdap1^{-/-}$ eMNs, we observed an increase in the length and area of the mitochondria in the axons (Fig. 1b), and altered mitochondrial mobility (Fig. 1c). Mitochondria mobility and travel distance were reduced in $Gdap1^{-/-}$ eMNs in both the anterograde and the retrograde movements (Fig. 1d, e). In addition, the frequency of pauses in the movement of mitochondria was higher in the anterograde transport in $Gdap1^{-/-}$ eMNs (Fig. 1f). No differences were found either in the frequency of pauses in retrograde movement (Fig. 1f) or the duration of the pauses in both movements (Fig. 1g). We also detected a reduction in the speed of retrograde transport in $Gdap1^{-/-}$ eMNs, while no differences were found in that of anterograde transport (Fig. 1h). These results indicate that GDAP1 deficiency causes larger mitochondria in the axons, which show mobility defects in both anterograde and retrograde movements.

3.2. GDAP1 deficiency is associated with ultrastructural abnormalities in mitochondrial cristae and defects in mitochondrial bioenergetics

Previous results in our group demonstrated that $Gdap1^{-/-}$ eMNs showed tubular mitochondria with altered cristae morphology (Barneo-Munoz et al., 2015). Here we have analyzed more deeply the mitochondrial and cristae ultrastructure. The morphology of the mitochondria in $Gdap1^{-/-}$ eMNs was abnormal, either elongated and tubular, or large and spherical (Fig. 2a). Quantification of cristae morphology revealed a significant increase of mitochondria with disorganized (ballooned and swollen) cristae in $Gdap1^{-/-}$ eMNs, compared to wild-type eMNs (Fig. 2b).

Since the disorganization of mitochondrial cristae is associated with impaired respiratory efficiency (Cogliati et al., 2013), we wondered if the loss of GDAP1 could also affect mitochondrial bioenergetic function. First, we analyzed the mitochondrial membrane potential ($\Delta\psi_m$) in eMNs by using the JC-1 ratiometric probe. We observed a lower $\Delta\psi_m$ in $Gdap1^{-/-}$ compared to the wild-type eMNs (Fig. 2c). Next, we analyzed mitochondrial respiration by measuring the oxygen consumption rate (OCR) in eMNs using the Seahorse XF-24 analyzer. We found a significant decrease in basal mitochondrial respiration as well as in ATP-linked respiration in $Gdap1^{-/-}$ eMNs (Fig. 2d, e). No differences were found in maximal uncoupled mitochondrial respiration, non-ATP linked respiration (proton leak) and non-mitochondrial respiration (Fig. 2d). To calculate ATP levels produced by mitochondrial respiration, we measured total intracellular ATP in control conditions or the presence of the F1-F0-ATP synthase inhibitor oligomycin. We found that ATP arising in mitochondria (i,e, oligomycin sensitive) was significantly reduced in $Gdap1^{-/-}$ eMNs (Fig. 2f). However, the maximal respiratory capacity of $Gdap1^{-/-}$ eMNs was not changed, suggesting that the respiratory chain itself was not grossly compromised. Altogether these results show GDAP1 deficiency associates with structural and functional mitochondria membrane abnormalities with a drop in ATP production and a deteriorated bioenergetics status in eMNs.

3.3. Loss of GDAP1 increases intracellular Ca^{2+}, affects mitochondria–ER membrane contacts and induces ER-stress

We further investigated the impact of the lack of GDAP1 in Ca^{2+} handling in eMNs. Quantification of basal $[Ca^{2+}]_{cyt}$ levels revealed a significant increase in $Gdap1^{-/-}$ eMNs (150 nM), when compared to wild-type eMNs (80 nM) (Fig. 3a). The normal range of intracellular free Ca^{2+} in resting neurons is 100 nM. The $Gdap1^{-/-}$ eMNs Ca^{2+} increment is reminiscent of that previously observed in $GDAP1$ knock-down SH-SY5Y cells (Pla-Martin et al., 2013). Moreover, $Gdap1^{-/-}$ eMNs exhibited axonal swelling and spheroids formation that retained a high intra-axonal Ca^{2+} level (Fig. 3a).

As GDAP1 is resident at MAMs, silencing $GDAP1$ reduces mitochondria-ER contacts (Pla-Martin et al., 2013) and membrane contacts provide a platform for Ca^{2+} homeostasis (Patergnani et al., 2011), we examined ER-mitochondria juxtaposition in cultured eMNs. We found a decrease in the number of contacts between these organelles in $Gdap1^{-/-}$ eMNs (Fig. 3b). We also quantified the expression levels of ER stress markers. Under basal conditions, we observed a significant increase of phosphorylated eukaryotic initiation factor 2α (eIF2α), which is critical in the regulation of protein synthesis during ER stress, and the ER chaperones immunoglobulin binding protein BiP and 94 kDa glucose-regulated protein (GRP94) in $Gdap1^{-/-}$ eMNs (Fig. 3c). After prolonged ER stress induction by thapsigargin treatment of eMNs we found a significant increase of C/EBP homologous protein (CHOP) in $Gdap1^{-/-}$ eMNs while eIF2α and GRP94 increases were equivalent for the two genotypes, likely by a ceiling effect (Fig. 3c). These results demonstrate that the loss of GDAP1 induces the increase of Ca^{2+} levels and ER stress in the soma and axons associated with MAMs defects in eMNs.

As the efficient transfer of Ca^{2+} from ER to mitochondria occurs in MAMs (Patergnani et al., 2011) we further investigated the stimulation of mitochondrial respiration in response to agents evoking the release of ER-Ca^{2+} in $Gdap1^{-/-}$ eMNs. OCR after treatment with 100 μm ATP (Fig. 4a) or 250 μm carbachol (Ccb, Fig. 4b), which mobilize ER-Ca^{2+} through activation of inositol 1,4,5-triphosphate (IP$_3$)-receptor (IP$_3$R) (Majumder et al., 2007; Van Acker et al., 2002), showed a small reduction in $Gdap1^{-/-}$ eMNs (~ 6 or 1% of basal values, respectively), but not significant differences between genotypes were observed (Fig. 4a, b), as previously found in brain neurons (Llorente-Folch et al., 2013; Rueda et al., 2015). These results indicate that the stimulation of mitochondrial respiration, in response to ER-Ca^{2+} mobilization, is not altered in $Gdap1^{-/-}$ eMNs, suggesting that MAMs defects due to GDAP1 deficiency do not affect stimulation of OXPHOS by ER-Ca^{2+} mobilizing agents, at least in response to these relatively small workloads.

3.4. Loss of GDAP1 impairs the response to the excitatory neurotransmitter glutamate

Next, we studied in eMNs the response to a more robust Ca^{2+} workload induced by glutamate, which is the excitatory neurotransmitter of MNs (Ramirez-Jarquin and Tapia, 2018). In eMNs, we observed that cytosolic Ca^{2+} transients elicited by glutamate were much larger than those triggered by ER-Ca^{2+} mobilization, and they returned to basal values during glutamate washout (Fig. 5a-f). The comparison between $Gdap1^{-/-}$ and wild-type eMNs did not show differences in the cytosolic Ca^{2+} response to glutamate normalized to the initial values nor in the amplitude of glutamate-evoked cytosolic Ca^{2+} transients (Fig. 5a, c). However, the half time decay of $[Ca^{2+}]_{cyt}$ to basal levels was significantly longer in $Gdap1^{-/-}$ eMNs (P: 3.03×10^{-8})(Fig. 5a, d). Indeed, several $Gdap1^{-/-}$ eMNs were not able to restore their basal $[Ca^{2+}]_{cyt}$ levels after excitatory stimulation, maintaining high $[Ca^{2+}]_{cyt}$ in soma, axons, and axonal swelling and spheroids (Fig. 5b).

We then investigated glutamate-induced stimulation of respiration. This agonist acts on various receptor types (Ramirez-Jarquin and Tapia, 2018) and induces a potent increase in workload mainly due to the entry of Na$^+$ (Llorente-Folch et al., 2016; Rueda et al., 2015). Consistent with the larger workload, the increase in respiration, about 75%, over basal values (Fig. 5e, f), is much more pronounced than that induced by ATP or CCh (Fig. 4). Despite similar glutamate-induced increases in $[Ca^{2+}]_{cyt}$ in $Gdap1^{-/-}$ or wild-type eMNs, glutamate-stimulation of respiration
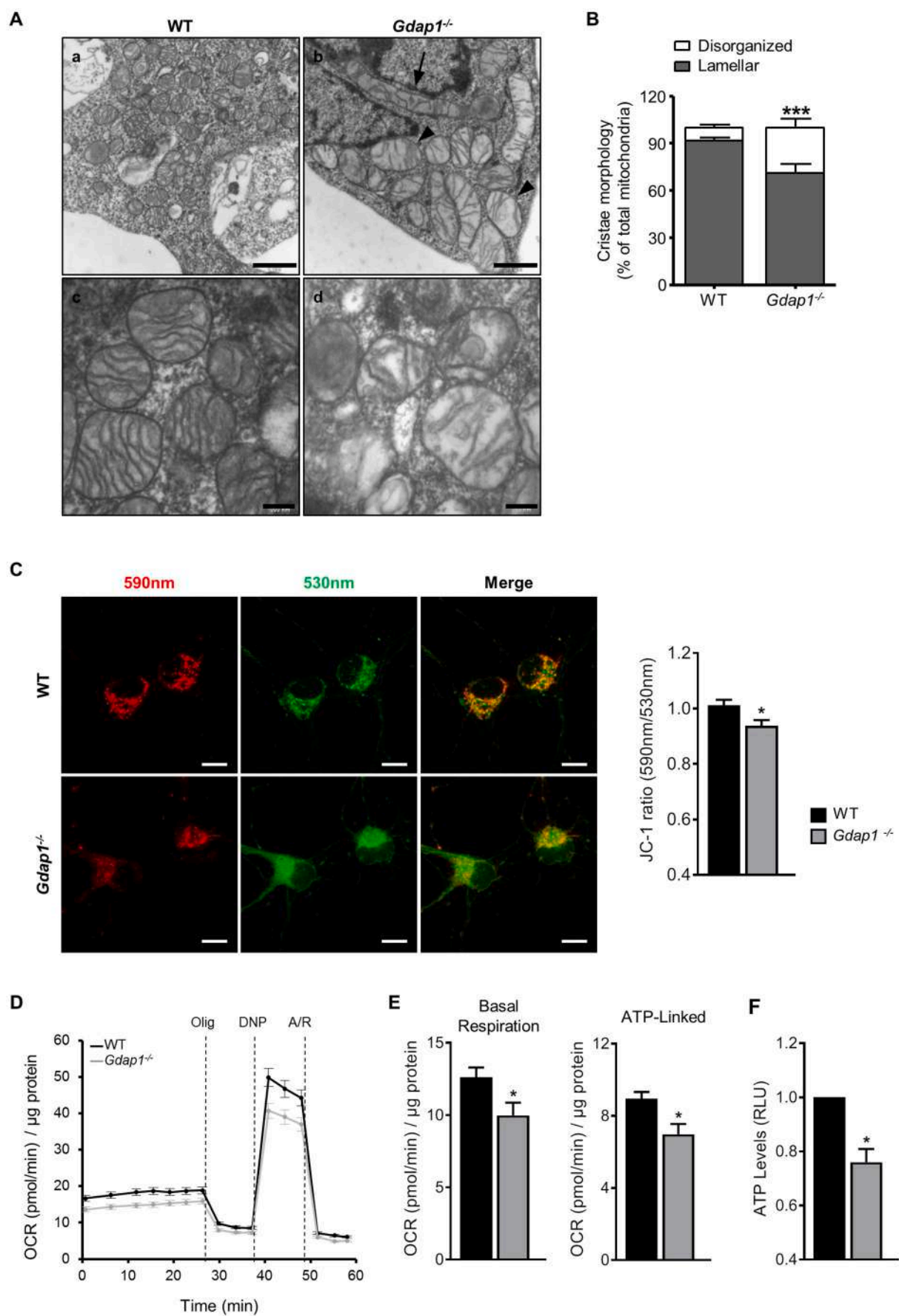
(caption on next page)

Fig. 2. GDAP1-deficient eMNs showed mitochondrial morphology and ultrastructure and impaired mitochondrial bioenergetic function. (A) Representative low-magnification (a, b) and high-magnification (c, d) electron transmission microscopy images of mitochondria in WT (a, c) and $Gdap1^{-/-}$ (b, d) eMNs. $Gdap1^{-/-}$ eMNs showed elongated tubular mitochondria (arrow in b) and enlarger spherical mitochondria (arrowheads in b) with disrupted cristae. (B) Quantification of cristae morphology in control and $Gdap1^{-/-}$ MNs. Approximately 30% of mitochondria exhibited disorganized cristae in $Gdap1^{-/-}$ MNs compared to 8% mitochondria in WT MNs. 60 eMNs were analyzed per genotype from three independent experiments. Scale bars: 1 μm (a, b) and 200 nm (c, d). (C) The panel shows representative images of mitochondrial membrane potential ($\Delta\psi_m$) staining of JC-1 in eMNs. Red (590 nm) and green (530 nm) fluorescence indicate high and low $\Delta\psi_m$, respectively. Quantitative analysis of JC-1 fluorescence intensity (red/green ratio) revealed a reduction of $\Delta\psi_m$ in $Gdap1^{-/-}$ eMNs. 251 WT and 215 $Gdap1^{-/-}$ eMNs were measured from three independent experiments. Scale bars: 10 μm. (D) Oxygen consumption rate (OCR) profile in WT and $Gdap1^{-/-}$ eMNs showing the sequential injection of metabolic inhibitors: 6 μM oligomycin (Olig), 1.6 mM 2,4-dinitrophenol (DNP) and 1 μM antimycin A/1 μM rotenone (A/R) at different time points (indicated by dashed lines), which allows the determination of basal oxygen consumption, oxygen consumption linked to ATP synthesis, non-ATP linked oxygen consumption (proton leak), maximal mitochondrial uncoupled respiration and non-mitochondrial respiration. (E) Quantification of basal mitochondrial OCR and ATP-linked OCR, which were significantly reduced in $Gdap1^{-/-}$ eMNs. (F) Quantification of ATP levels produced by mitochondrial respiration showing reduced levels in $Gdap1^{-/-}$ eMNs. Results are expressed as mean ± SEM of three different experiments. *p ≤ 0.05, ***p ≤ 0.001. RLU, relative luminescence units.

was lower in $Gdap1^{-/-}$ eMNs (Fig. 5e, f). These results show that the basal bioenergetics failure (Fig. 2) jeopardizes a full respiratory response to the large workload induced by glutamate, and prevents a rapid return of $[Ca^{2+}]_{cyt}$ to basal levels during glutamate washout.

The Ca^{2+} signals elicited in response to glutamate mainly arise from calcium entry along with ionotropic glutamate receptors but also ER-Ca^{2+}, via Ca^{2+}-induced Ca^{2+} activation ryanodine receptors (RyR) (Meissner, 2002). To analyze whether GDAP1 deficiency affected the respiratory response to ER-Ca^{2+} release via RyR, we employed N-methyl-D-aspartate (NMDA), as activation of NMDA receptors results in Ca^{2+}-induced Ca^{2+}-release from RyR (Ruiz et al., 2009). The involvement of RyR in the response to NMDA was determined by treatment with dantrolene, a specific inhibitor of RyR (Ruiz et al., 2009). Fig. 5, panels g and h, show that NMDA-induced OCR stimulation decreased by exposure to dandrolene, indicating the participation of Ca^{2+}-induced Ca^{2+} release via RyR, both in wild-type and $Gdap1^{-/-}$ eMNs. RyR-dependent OCR stimulation was calculated from the difference between NMDA-stimulation of OCR in the absence or presence of dantrolene (Fig. 5g). We did not observe any difference between wild-type and $Gdap1^{-/-}$ eMNs.

These results rule out a specific involvement of ER-to-mitochondria Ca^{2+} signaling in the deficient respiratory responses to glutamate agonists in $Gdap1^{-/-}$ eMNs. Rather, the bioenergetics failure revealed from the lower basal OCR in GDAP1-deficient eMNs points to a general impairment of the respiratory response to high workloads as imposed by glutamate. The positioning of mitochondria away from the cell body at sites where an intense stimulation of ATP production by OXPHOS is required (PMCA and Na^+ pumps in the plasma membrane), appears to be perturbed in GDAP1 deficiency due to the defects in mitochondrial movement, contributing to this impairment.

4. Discussion

Here we report that the absence of GDAP1 in cultured murine eMNs causes morphological and functional mitochondria defects which could explain GDAP1-related CMT axonopathy. We previously described that GDAP1 is located at MAMs and the mitochondria–ER–plasmatic membrane contacts (Ca^{2+} microdomains), and that membrane contact sites are affected by GDAP1 depletion (Barneo-Munoz et al., 2015; Pla-Martin et al., 2013). Now we found there is defective mitochondrial trafficking associated with a notable energetic impairment and abnormal Ca^{2+} handling that correlate with abnormal glutamate response and presynaptic dysfunction in eMNs.

Mitochondria defective in GDAP1 showed movement reduction and changes in both anterograde and retrograde traffic, which could compromise this organelle to reach the synaptic terminal and be back to the soma, respectively. The mitochondrial movement was slower in retrograde transport but more interrupted and paused in anterograde transport in $Gdap1^{-/-}$ axons. Mitochondria pausing in anterograde transport has been previously observed in another model of $Gdap1$-null mice (Niemann et al., 2014). The molecular mechanism for pausing is related to the elevation of cytosolic Ca^{2+} (Saotome et al., 2008), a

phenomenon that we have observed in the $Gdap1^{-/-}$ eMNs. Our results also showed a clear effect of GDAP1 absence on the mitochondrial morphology. $Gdap1^{-/-}$ eMNs showed elongated mitochondria and mitochondrial spheroids formation, which are two morphological patterns of mitochondrial decline by fission defects (Ishihara et al., 2009; Wakabayashi et al., 2009). We also observed in $Gdap1^{-/-}$ eMNs ultrastructure defects of the mitochondrial cristae that are known to affect mitochondrial function and bioenergetics capacity (Cogliati et al., 2013). Indeed, we have detected a global mitochondrial bioenergetic dysfunction in $Gdap1^{-/-}$ eMNs with a reduction in mitochondrial membrane potential, basal mitochondrial respiration and mitochondrial respiration linked to ATP synthesis, which affects mitochondrial ATP synthesis. These findings are in agreement with both bioenergetics defects in the peripheral nerves of our $Gdap1^{-/-}$ mice (Barneo-Munoz et al., 2015), and decreased respiratory chain complex I activity (Cassereau et al., 2011) and reduced mitochondrial membrane potential (Noack et al., 2012) in fibroblasts from CMT-$GDAP1$ patients. The reduction of mitochondrial fission could also impair mitochondrial bioenergetics through the accumulation of oxidative damage that affects morphology and decreased respiratory functions (Kageyama et al., 2012). Moreover, in $Gdap1^{-/-}$ eMNs we have recently shown an excess of reactive oxygen species (ROS) and mitochondrial superoxide (Fernandez-Lizarbe et al., 2019), which agree with the oxidative stress previously suggested in patients' fibroblasts (Noack et al., 2012), mouse (Niemann et al., 2014) and $Drosophila$ (Lopez Del Amo et al., 2015).

In this study, we also found high intra-axonal Ca^{2+} levels in $Gdap1^{-/-}$ eMNs, which could affect the mitochondrial axonal transport. Increases in resting $[Ca^{2+}]_{cyt}$ in neurons occur in physiological aging and pathological conditions (Jiang et al., 2012; Woolums et al., 2020). This scenario could lead to a decrease in healthy mitochondria and the accumulation of damaged mitochondria, which could affect the proper location of the organelle in distal high metabolic demanding regions, compromising synaptic function and therefore axonal integrity. This hypothesis may explain, at least in part, why the distal portions of the peripheral nerves are principally affected in CMT disease involving $GDAP1$ mutations (Sevilla et al., 2008). Other parameters apart from high Ca^{2+} levels and mitochondrial size could disrupt mitochondria axonal transport. Previous results showed that GDAP1 α-loop domain interacts with β-tubulin, and recessive $GDAP1$ mutations inside this α-loop induce abnormal mitochondrial localization but do not have any effect on mitochondrial fission (Gonzalez-Sanchez et al., 2017; Niemann et al., 2005). These findings suggest that lack of GDAP1 could interfere in mitochondrial anchoring to microtubules leading to defective mitochondrial axonal transport, as it has been similarly reported in $MFN2$ mutations (Singaravelu et al., 2011). In addition, ATP decrease detected in $Gdap1^{-/-}$ eMNs could also be affecting mitochondrial mobility (Zala et al., 2013). Thus, multiple pathological processes might be contributing to the defective mitochondrial transport in $Gdap1^{-/-}$ axons causing a synaptic dysfunction, which may be a common pathophysiological process in CMT since it has also been described in other CMT neuropathies (Pareyson et al., 2015).

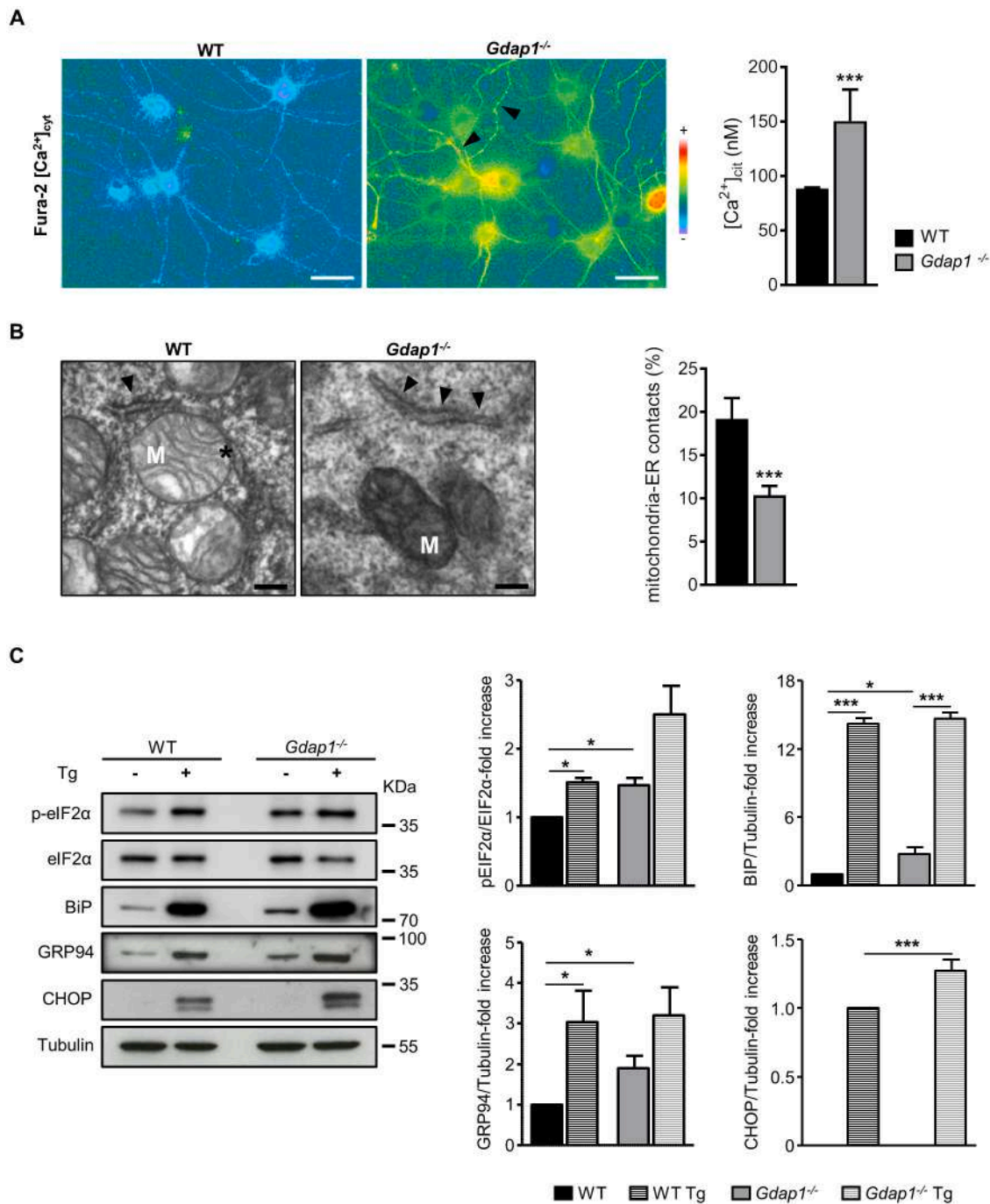The absence of GDAP1 may have a strong effect on the physiology of

Fig. 3. Deficiency of GDAP1 increases $[Ca^{2+}]_{cyt}$, reduces mitochondria-ER contacts and induces ER-stress in eMNs. (A) $[Ca^{2+}]_{cyt}$ determined by Fura-2 AM ratio imaging was significantly higher in $Gdap1^{-/-}$ eMNs than in WT MNs. $Gdap1^{-/-}$ eMNs showed axonal spheroids contained high Ca^{2+} levels (arrowheads). 369 WT and 456 $Gdap1^{-/-}$ eMNs were analyzed from five independent experiments. (B) Representative electron transmission microscopy images of ER-mitochondria contacts in WT and $Gdap1^{-/-}$ eMNs. Arrowheads indicate ER, M indicates mitochondria and asterisk indicates mitochondria in contact with ER. (C) Quantification of mitochondria-ER contacts percentage in WT and $Gdap1^{-/-}$ eMNs showed a reduction of these contacts in the absence of GDAP1. 100 WT and $Gdap1^{-/-}$ eMNs were analyzed from three independent experiments. (D) Immunodetection and (E) densitometric quantifications of phosphorylated eIF2α (p-eIF2α), eIF2α, BiP, GRP94 and CHOP in wild-type and $Gdap1^{-/-}$ eMNs untreated and treated with 0.1 μm thapsigargin (Tg) for 18 h. Densitometry of bands expressed relative to controls (100%) show significantly increased levels of p-eIF2α, BiP and GRP94 in $Gdap1^{-/-}$ eMNs untreated. No significant differences between them were observed after Tg treatment (p-eIF2α, $p = 0.16$; BiP, $p = 0.8$; GRP94, $p = 0.27$), but CHOP expression was significantly higher in $Gdap1^{-/-}$ than wild-type eMNs treated. Results are from four independent experiments. Data are expressed as mean ± SEM. *$p < 0.05$; ***$p < 0.001$. Scale bars: 200 nm.

eMNs in the $Gdap1^{-/-}$ mouse by (i) significant increase in $[Ca^{2+}]_{cyt}$ levels in eMNs, which are cells especially sensitive to an excessive influx of Ca^{2+} as they express low level of Ca^{2+} buffer proteins (Van Den Bosch et al., 2006), and (ii) high levels of Ca^{2+}–permeable α-amino-5-methyl-3-hydroxisoxazolone-4-propionate (AMPA) receptors lacking the GluR2 subunit which makes them vulnerable to excitotoxicity (Williams et al., 1997). In $Gdap1^{-/-}$ eMNs, the cytosolic Ca^{2+} transient amplitude during glutamate-evoked physiological stimulation was not altered. However, Ca^{2+} clearance after neuronal stimulation was slower in $Gdap1^{-/-}$ eMNs, which might be a consequence of a defective Ca^{2+} buffering
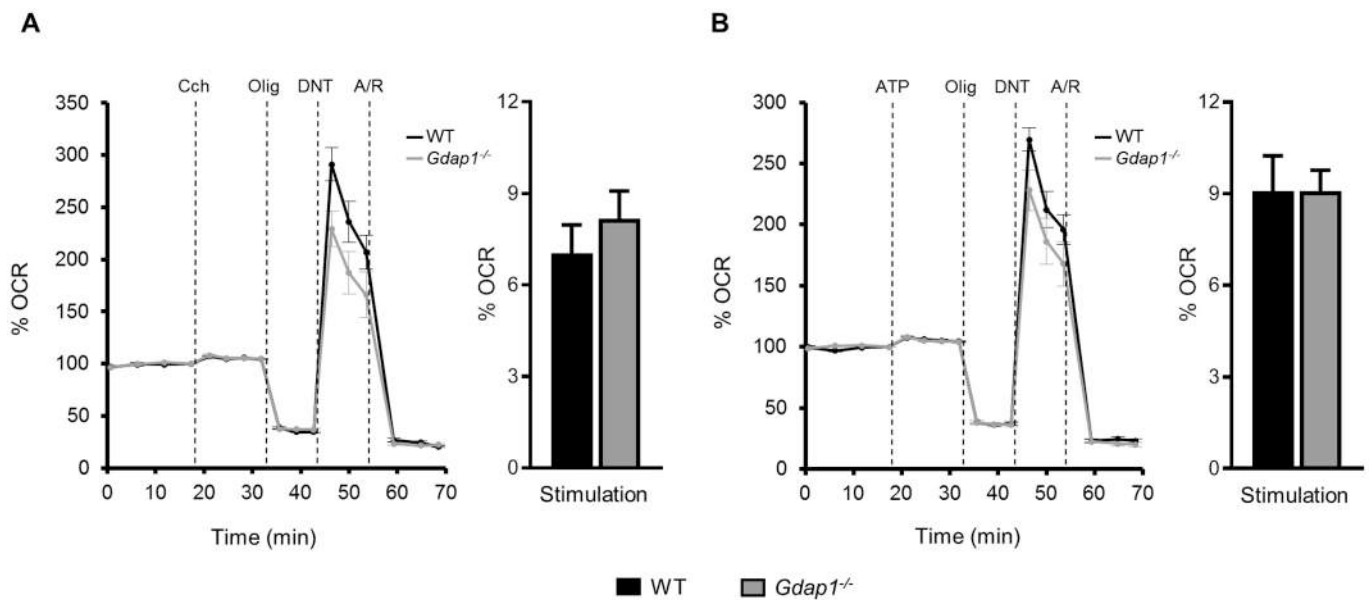
Fig. 4. OCR in response to ER-Ca^{2+} release is not affected in GDAP1-deficient MNs. Profile of ER-Ca^2-stimulation of mitochondrial respiration and quantification of OCR stimulation. Oxygen consumption rate expressed as a percentage of OCR after the addition of (A) 250 μM Carbachol (Cch) and (B) 100 μM ATP in the absence and presence of 10 μM dantrolene. Data are expressed as mean ± SEM from three independent experiments.

ability in GDAP1-lacking mitochondria, or deficient Ca^{2+} extrusion. These findings are also supported by the reduction in glutamate-stimulated mitochondrial respiration that we found in Gdap1$^{-/-}$ MNs, since the respiratory response to the high workload imposed by this neurotransmitter is regulated by Ca^{2+} (Llorente-Folch et al., 2016; Rueda et al., 2016). Importantly, this diminished Ca^{2+} dependent-mitochondrial respiration could lead to a reduction of mitochondrial ATP production during synaptic transmission, which is known to be essential for the regulation of synaptic activity (Vos et al., 2010). The calmodulin (CaM)-activated plasma membrane Ca^{2+}-ATPase or PMCA is the major high affinity, low-capacity Ca^{2+} extrusion system at the plasma membrane, and decreases in its activity account for increases in resting [Ca^{2+}]$_{cyt}$ (Jiang et al., 2012). Thus, the fall in ATP levels found in Gdap1$^{-/-}$ eMNs may limit PMCA activity and underlie their increase in [Ca^{2+}]$_{cyt}$. Since Ca^{2+} ions also regulate the neurotransmission process (Medler and Gleason, 2002; Vos et al., 2010), we propose that the defects in Ca^{2+} handling and mitochondrial ATP production observed in Gdap1$^{-/-}$ eMNs could eventually dysregulate neurotransmitter release and, consequently, synaptic transmission in GDAP1-associated CMT disease.

Several reasons suggest that mitochondrial Ca^{2+} buffering after physiological glutamate stimulation is impaired in GDAP1-deficient MNs. One possible explanation would be that the depolarization of mitochondria impairs the ability of these organelles to sequester excess Ca^{2+}, which, in turn, may expose cytosol to higher Ca^{2+} concentrations after excitatory stimulation. Pharmacological depolarization of mitochondria results in a marked slowing of cytosolic Ca^{2+} recovery after electrical stimulation in DRG neurons (Shutov et al., 2013). On the other hand, the defective axonal mitochondrial movement found in Gdap1$^{-/-}$ eMNs might affect the correct mitochondrial localization at synaptic terminals, where there would be a reduced pool of mitochondria to deal with Ca^{2+} clearance during neuronal stimulation. Accordingly, it has been shown that the absence of mitochondrial in axon terminals drastically alters Ca^{2+} transients and reduces ATP supplies, leading to an aberrant synaptic transmission (Ma et al., 2009; Stowers et al., 2002). Therefore, based on these results, it could be proposed that the impairment in Ca^{2+} signaling during neuronal stimulation in Gdap1$^{-/-}$ eMNs could disrupt neurotransmission at the neuromuscular junction leading to synaptic dysfunction and resulting in axonal degeneration.

This hypothesis is supported by the abnormalities in neuromuscular junction structures we have previously observed in the Gdap1$^{-/-}$ mice (Barneo-Munoz et al., 2015).

In addition to altering mitochondrial transport and function, GDAP1 deficiency also disrupts the relationship between mitochondria and ER. We have observed loss of contacts between both organelles in the absence of GDAP1, as previously documented in other GDAP1-lacking models (Lopez Del Amo et al., 2017; Pla-Martin et al., 2013) as well as an increase in ER stress activation. Accordingly, the deletion/mutation of other MAMs protein-coding genes have been shown to disrupt ER-mitochondria interactions and induce ER-stress (Berthet et al., 2014; de Brito and Scorrano, 2008). Moreover, the reduction in ER-mitochondria contacts could also be altering the regulation of mitochondrial dynamics in GDAP1-deficient MNs, since ER tubules are involved in marking the sites of mitochondrial fission (Friedman et al., 2011). Thus, since GDAP1 does not seem to be a canonical fission protein (Niemann et al., 2005), GDAP1 might regulate mitochondrial fission by promoting or modulating the formation of ER-mitochondria contacts.

Besides participation in mitochondrial morphology, MAMs also play a key role in mitochondrial bioenergetics by regulating Ca^{2+} exchange between both organelles. The close apposition of the ER with mitochondria is crucial to mediate a correct Ca^{2+} transfer from ER to mitochondria, which is required for efficient mitochondrial respiration and ATP production (Patergnani et al., 2011). However, although GDAP1 deficiency produced the loss of ER-mitochondria contacts, mitochondrial respiration in response to ER-Ca^{2+} release was not affected, suggesting that mitochondrial Ca^{2+} handling of ER-Ca^{2+} is not altered. In agreement with our results in eMNs, no differences were found in mitochondrial Ca^{2+} uptake in response to ER-Ca^{2+} mobilization in GDAP1-silenced cells (Pla-Martin et al., 2013). Altogether, these findings suggest that the mitochondrial bioenergetic dysfunction found in Gdap1$^{-/-}$ eMNs is mainly associated with mitochondrial morphology and functional abnormalities and not with the ER-mitochondrial uncoupling.

In conclusion, we provide evidence of the key role of GDAP1 in maintaining proper mitochondrial function and its consequences for the correct neuronal and axonal physiology. We propose that defects in the mitochondrial movement across the axon, bioenergetics and Ca^{2+} handling affect important functions in the axonal and synaptic biology
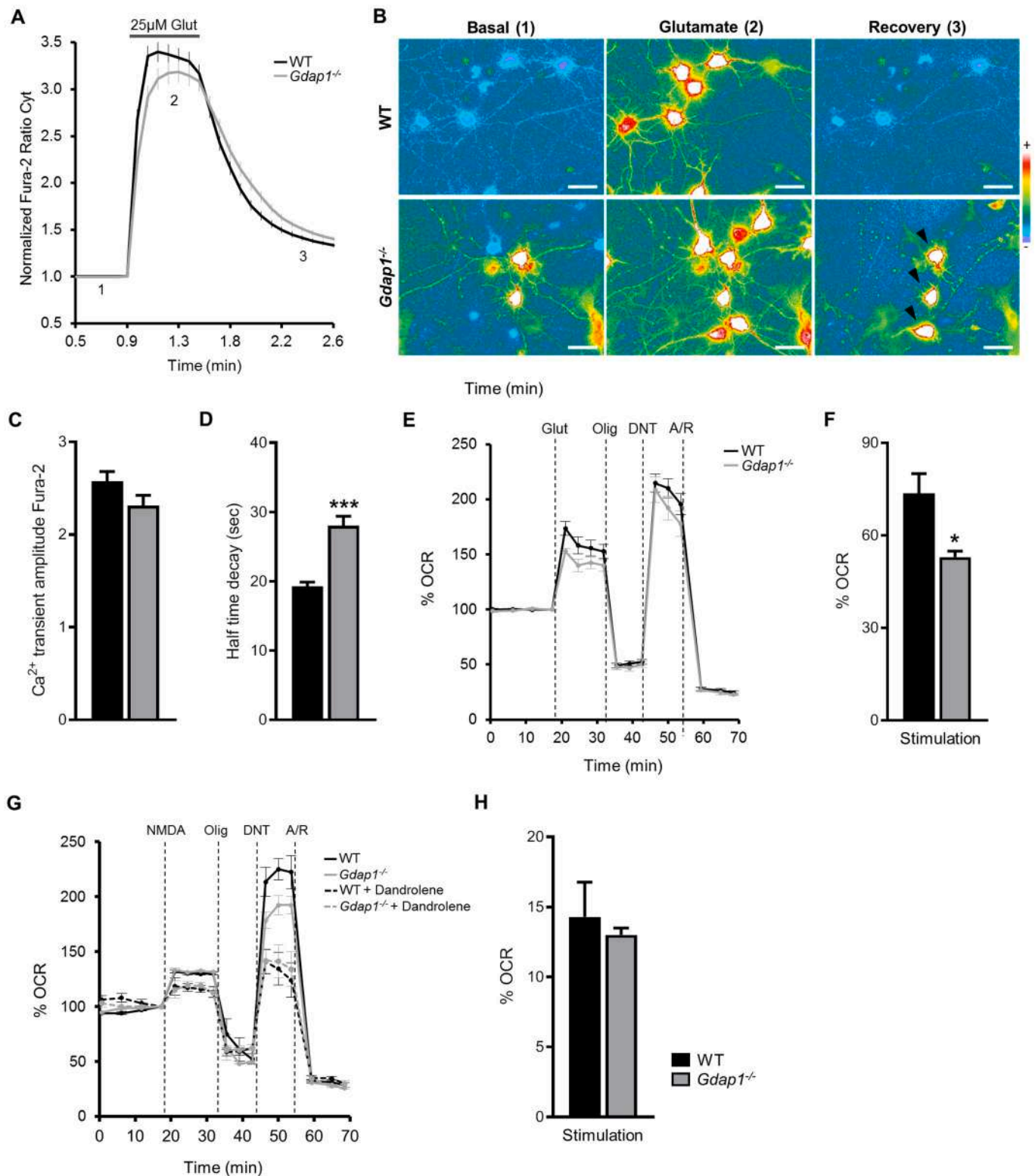
Fig. 5. Loss of GDAP1 affects Ca^{2+} handling and respiration in response to glutamate. (A) Glutamate-evoked cytosolic Ca^{2+} transient monitored by Fura-2 AM ratio imaging in WT and $Gdap1^{-/-}$ eMNs. (B) Images of $[Ca^{2+}]_{cyt}$ determined by Fura-2 AM ratio in eMNs of both genotypes after glutamate treatment and washout. (C) No significant difference was found in the amplitude of Ca^{2+} transient ($p = 0.08$), (D) but the half time decay of Ca^{2+} transient (50% of return to basal level) was longer in $Gdap1^{-/-}$ eMNs. Some $Gdap1^{-/-}$ eMNs maintained high cytosolic Ca^{2+} levels after glutamate stimulation (arrows). 112 WT and 107 $Gdap1^{-/-}$ eMNs were analyzed from three independent experiments. (E) Profile of glutamate-stimulation of mitochondrial respiration. Oxygen consumption rate is expressed as a percentage of OCR after glutamate addition. (F) Quantification of % OCR stimulation showed that OCR response to glutamate was lower in $Gdap1^{-/-}$ than in WT eMNs. Results are from five independent experiments. Data are expressed as mean ± SEM. *$p \leq 0.05$, ***$p \leq 0.001$. Scale bar: 20 µm. (G) Effect of dandrolene on NMDA-stimulation of mitochondrial respiration. Neurons were incubated with or without 10 µM dandrolene and 25 µM NMDA was added as indicated. (H) Quantification dandrelene-sensitive NMDA-stimulatiom of OCR as the difference between OCR stimulation in the absence or presence of 10 µM dandrolene. Data are expressed as mean ± SEM from three independent experiments. *$p \leq 0.05$, ***$p \leq 0.001$. Scale bar: 20 µm.

as major pathogenic mechanisms in the pathophysiology of *GDAP1*-related CMT, which open new cellular and molecular druggable targets in genetic neuropathies.

Supplementary data to this article can be found online at https://doi.org/10.1016/j.nbd.2021.105300.

Funding

Declaration of Competing Interest

The authors declare that there are no competing interests.

References

Baloh, R.H., et al., 2007. Altered axonal mitochondrial transport in the pathogenesis of Charcot-Marie-Tooth disease from mitofusin 2 mutations. J. Neurosci. 27, 422–430. https://doi.org/10.1523/JNEUROSCI.4798-06.2007.

Barneo-Munoz, M., et al., 2015. Lack of GDAP1 induces neuronal calcium and mitochondrial defects in a knockout mouse model of Charcot-Marie-Tooth neuropathy. PLoS Genet. 11, e1005115 https://doi.org/10.1371/journal.pgen.1005115.

Baxter, R.V., et al., 2002. Ganglioside-induced differentiation-associated protein-1 is mutant in Charcot-Marie-Tooth disease type 4A/8q21. Nat. Genet. 30, 21–22. https://doi.org/10.1038/ng796.

Berthet, A., et al., 2014. Loss of mitochondrial fission depletes axonal mitochondria in midbrain dopamine neurons. J. Neurosci. 34, 14304–14317. https://doi.org/10.1523/JNEUROSCI.0930-14.2014.

Brini, M., et al., 2014. Neuronal calcium signaling: function and dysfunction. Cell. Mol. Life Sci. 71, 2787–2814. https://doi.org/10.1007/s00018-013-1550-7.

Cantarero, L., et al., 2020. Mitochondria–lysosome membrane contacts are defective in *GDAP1*-related Charcot-Marie-Tooth disease. Hum. Mol. Genet. 29, 3589–3605. https://doi.org/10.1093/hmg/ddaa243.

Cassereau, J., et al., 2011. Mitochondrial dysfunction and pathophysiology of Charcot-Marie-Tooth disease involving GDAP1 mutations. Exp. Neurol. 227, 31–41. https://doi.org/10.1016/j.expneurol.2010.09.006.

Claramunt, R., et al., 2005. Genetics of Charcot-Marie-Tooth disease type 4A: mutations, inheritance, phenotypic variability, and founder effect. J. Med. Genet. 42, 358–365. https://doi.org/10.1136/jmg.2004.022178.

Cogliati, S., et al., 2013. Mitochondrial cristae shape determines respiratory chain supercomplexes assembly and respiratory efficiency. Cell 155, 160–171. https://doi.org/10.1016/j.cell.2013.08.032.

Cuesta, A., et al., 2002. The gene encoding ganglioside-induced differentiation-associated protein 1 is mutated in axonal Charcot-Marie-Tooth type 4A disease. Nat. Genet. 30, 22–25. https://doi.org/10.1038/ng798.

de Brito, O.M., Scorrano, L., 2008. Mitofusin 2 tethers endoplasmic reticulum to mitochondria. Nature 456, 605–610. https://doi.org/10.1038/nature07534.

Denton, R.M., 2009. Regulation of mitochondrial dehydrogenases by calcium ions. Biochim. Biophys. Acta 1787, 1309–1316. https://doi.org/10.1016/j.bbabio.2009.01.005.

Devine, M.J., Kittler, J.T., 2018. Mitochondria at the neuronal presynapse in health and disease. Nat. Rev. Neurosci. 19, 63–80. https://doi.org/10.1038/nrn.2017.170.

Fernandez-Lizarbe, S., et al., 2019. Neuroinflammation in the pathogenesis of axonal Charcot-Marie-Tooth disease caused by lack of GDAP1. Exp. Neurol. 320, 113004 https://doi.org/10.1016/j.expneurol.2019.113004.

Friedman, J.R., et al., 2011. ER tubules mark sites of mitochondrial division. Science 334, 358–362. https://doi.org/10.1126/science.1207385.

Gingras, M., et al., 2007. Optimized protocols for isolation of primary motor neurons, astrocytes and microglia from embryonic mouse spinal cord. J. Neurosci. Methods 163, 111–118. https://doi.org/10.1016/j.jneumeth.2007.02.024.

Glancy, B., Balaban, R.S., 2012. Role of mitochondrial Ca2+ in the regulation of cellular energetics. Biochemistry 51, 2959–2973. https://doi.org/10.1021/bi2018909.

Gonzalez-Sanchez, P., et al., 2017. CMT-linked loss-of-function mutations in GDAP1 impair store-operated Ca(2+) entry-stimulated respiration. Sci. Rep. 7, 42993 https://doi.org/10.1038/srep42993.

Grynkiewicz, G., et al., 1985. A new generation of Ca2+ indicators with greatly improved fluorescence properties. J. Biol. Chem. 260, 3440–3450.

Ishihara, N., et al., 2009. Mitochondrial fission factor Drp1 is essential for embryonic development and synapse formation in mice. Nat. Cell Biol. 11, 958–966. https://doi.org/10.1038/ncb1907.

Jiang, L., et al., 2012. Decreases in plasma membrane Ca(2)(+)-ATPase in brain synaptic membrane rafts from aged rats. J. Neurochem. 123, 689–699. https://doi.org/10.1111/j.1471-4159.2012.07918.x.

Kageyama, Y., et al., 2012. Mitochondrial division ensures the survival of postmitotic neurons by suppressing oxidative damage. J. Cell Biol. 197, 535–551. https://doi.org/10.1083/jcb.201110034.

Li, S., et al., 2020. The cross-talk of energy sensing and mitochondrial anchoring sustains synaptic efficacy by maintaining presynaptic metabolism. Nat. Metab. 2, 1077–1095. https://doi.org/10.1038/s42255-020-00289-0.

Lin, M.Y., Sheng, Z.H., 2015. Regulation of mitochondrial transport in neurons. Exp. Cell Res. 334, 35–44. https://doi.org/10.1016/j.yexcr.2015.01.004.

Llorente-Folch, I., et al., 2013. Calcium-regulation of mitochondrial respiration maintains ATP homeostasis and requires ARALAR/AGC1-malate aspartate shuttle in intact cortical neurons. J. Neurosci. 33, 13957–13971, 13971a. https://doi.org/10.1523/JNEUROSCI.0929-13.2013.

Llorente-Folch, I., et al., 2016. L-lactate-mediated neuroprotection against glutamate-induced excitotoxicity requires ARALAR/AGC1. J. Neurosci. 36, 4443–4456. https://doi.org/10.1523/JNEUROSCI.3691-15.2016.

Lopez Del Amo, V., et al., 2015. Mitochondrial defects and neuromuscular degeneration caused by altered expression of Drosophila Gdap1: implications for the Charcot-Marie-Tooth neuropathy. Hum. Mol. Genet. 24, 21–36. https://doi.org/10.1093/hmg/ddu416.

Lopez Del Amo, V., et al., 2017. A Drosophila model of GDAP1 function reveals the involvement of insulin signalling in the mitochondria-dependent neuromuscular degeneration. Biochim. Biophys. Acta Mol. basis Dis. 1863, 801–809. https://doi.org/10.1016/j.bbadis.2017.01.003.

Ma, H., et al., 2009. KIF5B motor adaptor syntabulin maintains synaptic transmission in sympathetic neurons. J. Neurosci. 29, 13019–13029. https://doi.org/10.1523/JNEUROSCI.2517-09.2009.

Majumder, P., et al., 2007. New insights into purinergic receptor signaling in neuronal differentiation, neuroprotection, and brain disorders. Purinergic Signal 3, 317–331. https://doi.org/10.1007/s11302-007-9074-y.

Marco, A., et al., 2004. Evolutionary and structural analyses of GDAP1, involved in Charcot-Marie-Tooth disease, characterize a novel class of glutathione transferase-related genes. Mol. Biol. Evol. 21, 176–187. https://doi.org/10.1093/molbev/msh013.

Medler, K., Gleason, E.L., 2002. Mitochondrial Ca(2+) buffering regulates synaptic transmission between retinal amacrine cells. J. Neurophysiol. 87, 1426–1439. https://doi.org/10.1152/jn.00627.2001.

Meissner, G., 2002. Regulation of mammalian ryanodine receptors. Front. Biosci. 7, d2072–d2080.

Naon, D., Scorrano, L., 2014. At the right distance: ER-mitochondria juxtaposition in cell life and death. Biochim. Biophys. Acta 1843, 2184–2194. https://doi.org/10.1016/j.bbamcr.2014.05.011.

Niemann, A., et al., 2005. Ganglioside-induced differentiation associated protein 1 is a regulator of the mitochondrial network: new implications for Charcot-Marie-Tooth disease. J. Cell Biol. 170, 1067–1078. https://doi.org/10.1083/jcb.200507087.

Niemann, A., et al., 2009. GDAP1 mutations differ in their effects on mitochondrial dynamics and apoptosis depending on the mode of inheritance. Neurobiol. Dis. 36, 509–520. https://doi.org/10.1016/j.nbd.2009.09.011.

Niemann, A., et al., 2014. The Gdap1 knockout mouse mechanistically links redox control to Charcot-Marie-Tooth disease. Brain 137, 668–682. https://doi.org/10.1093/brain/awt371.

Noack, R., et al., 2012. Charcot-Marie-Tooth disease CMT4A: GDAP1 increases cellular glutathione and the mitochondrial membrane potential. Hum. Mol. Genet. 21, 150–162. https://doi.org/10.1093/hmg/ddr450.

Pareyson, D., et al., 2015. Mitochondrial dynamics and inherited peripheral nerve diseases. Neurosci. Lett. 596, 66–77. https://doi.org/10.1016/j.neulet.2015.04.001.

Pareyson, D., et al., 2017. New developments in Charcot-Marie-Tooth neuropathy and related diseases. Curr. Opin. Neurol. 30, 471–480. https://doi.org/10.1097/WCO.0000000000000474.

Patergnani, S., et al., 2011. Calcium signaling around mitochondria associated membranes (MAMs). Cell Commun. Signal. 9, 19. https://doi.org/10.1186/1478-811X-9-19.

Pedrola, L., et al., 2005. GDAP1, the protein causing Charcot-Marie-Tooth disease type 4A, is expressed in neurons and is associated with mitochondria. Hum. Mol. Genet. 14, 1087–1094. https://doi.org/10.1093/hmg/ddi121.

Pla-Martin, D., et al., 2013. Silencing of the Charcot-Marie-Tooth disease-associated gene GDAP1 induces abnormal mitochondrial distribution and affects Ca2+ homeostasis by reducing store-operated Ca2+ entry. Neurobiol. Dis. 55, 140–151. https://doi.org/10.1016/j.nbd.2013.03.010.

Qian, W., Van Houten, B., 2010. Alterations in bioenergetics due to changes in mitochondrial DNA copy number. Methods 51, 452–457. https://doi.org/10.1016/j.ymeth.2010.03.006.

Ramirez-Jarquin, U.N., Tapia, R., 2018. Excitatory and inhibitory neuronal circuits in the spinal cord and their role in the control of motor neuron function and degeneration. ACS Chem. Neurosci. 9, 211–216. https://doi.org/10.1021/acschemneuro.7b00503.

Rossor, A.M., et al., 2013. Clinical implications of genetic advances in Charcot-Marie-Tooth disease. Nat. Rev. Neurol. 9, 562–571. https://doi.org/10.1038/nrneurol.2013.179.

Rueda, C.B., et al., 2015. Mitochondrial ATP-Mg/Pi carrier SCaMC-3/Slc25a23 counteracts PARP-1-dependent fall in mitochondrial ATP caused by excitotoxic insults in neurons. J. Neurosci. 35, 3566–3581. https://doi.org/10.1523/JNEUROSCI.2702-14.2015.

Rueda, C.B., et al., 2016. Glutamate excitotoxicity and Ca2+−regulation of respiration: Role of the Ca2+ activated mitochondrial transporters (CaMCs). Biochim. Biophys. Acta 1857, 1158–1166. https://doi.org/10.1016/j.bbabio.2016.04.003.

Ruiz, F., et al., 1998. Protection by pyruvate and malate against glutamate-mediated neurotoxicity. Neuroreport 9, 1277–1282.

Ruiz, A., et al., 2009. Endoplasmic reticulum Ca(2+) release through ryanodine and IP (3) receptors contributes to neuronal excitotoxicity. Cell Calcium 46, 273–281. https://doi.org/10.1016/j.ceca.2009.08.005.

Saotome, M., et al., 2008. Bidirectional Ca2+−dependent control of mitochondrial dynamics by the Miro GTPase. Proc. Natl. Acad. Sci. U. S. A. 105, 20728–20733. https://doi.org/10.1073/pnas.0808953105.

Satrustegui, J., et al., 2007. Mitochondrial transporters as novel targets for intracellular calcium signaling. Physiol. Rev. 87, 29–67. https://doi.org/10.1152/physrev.00005.2006.

Sevilla, T., et al., 2008. Vocal cord paresis and diaphragmatic dysfunction are severe and frequent symptoms of GDAP1-associated neuropathy. Brain. 131, 3051–3061. https://doi.org/10.1093/brain/awn228.

Shutov, L.P., et al., 2013. Mitochondria and plasma membrane Ca2+-ATPase control presynaptic Ca2+ clearance in capsaicin-sensitive rat sensory neurons. J. Physiol. 591, 2443–2462. https://doi.org/10.1113/jphysiol.2012.249219.

Singaravelu, K., et al., 2011. Mitofusin 2 regulates STIM1 migration from the Ca2+ store to the plasma membrane in cells with depolarized mitochondria. J. Biol. Chem. 286, 12189–12201. https://doi.org/10.1074/jbc.M110.174029.

Sivera, R., et al., 2010. Phenotypical features of the p.R120W mutation in the GDAP1 gene causing autosomal dominant Charcot-Marie-Tooth disease. J. Peripher. Nerv. Syst. 15, 334–344. https://doi.org/10.1111/j.1529-8027.2010.00286.x.

Soler, R.M., et al., 1998. Calmodulin is involved in membrane depolarization-mediated survival of motoneurons by phosphatidylinositol-3 kinase- and MAPK-independent pathways. J. Neurosci. 18, 1230–1239.

Southam, K.A., et al., 2013. Microfluidic primary culture model of the lower motor neuron-neuromuscular junction circuit. J. Neurosci. Methods 218, 164–169. https://doi.org/10.1016/j.jneumeth.2013.06.002.

Stowers, R.S., et al., 2002. Axonal transport of mitochondria to synapses depends on milton, a novel Drosophila protein. Neuron 36, 1063–1077.

Vallmitjana, A., et al., 2017. Motion estimation of subcellular structures from fluorescence microscopy images. Conf. Proc. IEEE Eng. Med. Biol. Soc. 4419–4422. https://doi.org/10.1109/EMBC.2017.8037836.

Van Acker, K., et al., 2002. IP(3)-mediated Ca(2+) signals in human neuroblastoma SH-SY5Y cells with exogenous overexpression of type 3 IP(3) receptor. Cell Calcium 32, 71–81.

Van Den Bosch, L., et al., 2006. The role of excitotoxicity in the pathogenesis of amyotrophic lateral sclerosis. Biochim. Biophys. Acta 1762, 1068–1082. https://doi.org/10.1016/j.bbadis.2006.05.002.

Voliani, V., et al., 2013. Orthogonal functionalisation of upconverting NaYF4 nanocrystals. Chemistry 19, 13538–13546. https://doi.org/10.1002/chem.201301353.

Vos, M., et al., 2010. Synaptic mitochondria in synaptic transmission and organization of vesicle pools in health and disease. Front Synaptic Neurosci. 2, 139. https://doi.org/10.3389/fnsyn.2010.00139.

Wakabayashi, J., et al., 2009. The dynamin-related GTPase Drp1 is required for embryonic and brain development in mice. J. Cell Biol. 186, 805–816. https://doi.org/10.1083/jcb.200903065.

Williams, T.L., et al., 1997. Calcium-permeable alpha-amino-3-hydroxy-5-methyl-4-isoxazole propionic acid receptors: a molecular determinant of selective vulnerability in amyotrophic lateral sclerosis. Ann. Neurol. 42, 200–207. https://doi.org/10.1002/ana.410420211.

Woolums, B.M., et al., 2020. TRPV4 disrupts mitochondrial transport and causes axonal degeneration via a CaMKII-dependent elevation of intracellular ca(2). Nat. Commun. 11, 2679. https://doi.org/10.1038/s41467-020-16411-5.

Zala, D., et al., 2013. Vesicular glycolysis provides on-board energy for fast axonal transport. Cell 152, 479–491. https://doi.org/10.1016/j.cell.2012.12.029.